

THE MECHANISM OF ENERGY TRANSFER IN TURBULENT POISEUILLE FLOW AT VERY LOW-REYNOLDS NUMVER

Koji Fukudome, Oaki Iida, Yasutaka Nagano

Department of Engineering Mechanics,

Nagoya Institute of Technology

Gokiso-cho, Showa-ku, Nagoya, Aichi, 466-8555, Japan

chd16505@stn.nitech.ac.jp, iida.oaki@nitech.ac.jp, nagano@heat.mech.nitech.ac.jp

ABSTRACT

Direct numerical simulations (DNSs) with a spectral method are performed to study structures of relaminarizing turbulent Poiseuille flow at very low-Reynolds numbers, where a flow, simultaneously including quasi-laminar and turbulent regions, becomes spatially intermittent. Turbulent energy is found to be exchanged between the turbulent and quasi-laminar regions; in the very vicinity of the wall, turbulent energy is transferred from the turbulent to quasi-laminar regions, while in the region away from the wall, it is transferred in the opposite direction. This energy exchange is attributed to the inclination of turbulent region with respect to streamwise direction in the plane parallel to the wall, and constant advection velocity of turbulent region over the entire channel. Moreover, we also confirmed generation of a large-scale flow circulating around the turbulent region, which continues to appear over the long time.

INTRODUCTION

Intermittent flow structure appears in various sheared flows at the very low-Reynolds numbers, and coined as turbulent-laminar pattern, which is confirmed by recent DNSs on relaminarizing turbulent Couette flow (Barkley et al., 2007) as well as relaminarizing turbulent Poiseuille flow (Tsukahara et al., 2007, Fukudome et al., 2008). Especially, in the study of Tsukahara et al.(2007), the turbulent-laminar patterns is found to be generated when the friction Reynolds number Re_τ defined by the channel half width and friction velocity becomes less than 80.

Moreover, in a previous study, the significant differences on turbulence statistics are observed between the quasi-laminar and turbulent flows. Iida et al. (1998) carried out DNSs of a Poiseuille flow at the friction Reynolds number 60 in the relatively small computational domain, where quasi-laminar and turbulent flows appear periodically with time, and showed that in the quasi-laminar flow, the sweep event, i.e., an inward motion of a high speed fluid toward a wall, attenuates and streamwise vortices very near the wall markedly disappear, though the vortices away from wall still remain. However, both quasi-laminar and turbulent flows are stably maintained, and laminar-turbulence pattern is generated in the large computational domain.

Clarifying the generation mechanism of a pattern must be important for understanding required conditions for

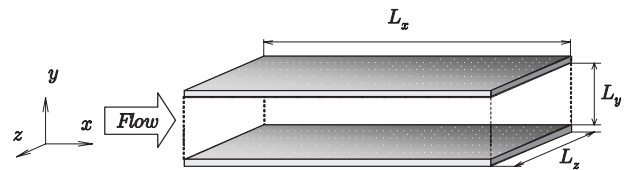


Figure 1: Flow configuration and coordinate system. transition to turbulence, which may gives us clues for methodology of controlling turbulence and keeping skin friction

at lower level. Moreover, it is also scientifically interesting to see how the large-scale asymmetric pattern is generated and maintained over the long period of time.

In this study, we perform direct numerical simulations of a turbulent Poiseuille flow at the very low-Reynolds number. As a result, it was confirmed that the unique pattern appears when Re_τ is around 60, which must be the transitional Reynolds number. Then, the entire flow is classified into quasi-laminar and turbulence regions by using the threshold value on streamwise vorticity, and turbulence statistics are spatially averaged in each region. Finally, a large-scale flow structure appearing over the long time is investigated in detail by averaging the turbulent region over time.

NUMERICAL PROCEDURES

The objective flow field is a channel flow shown in Fig.1, where x , y and z are set to be streamwise, wall-normal and span direction, respectively, The flow is driven by a constant mean pressure gradient in the x -direction, and assumed to be homogeneous in the x and z -directions, so that periodic boundary conditions are imposed in these directions. However, the no-slip boundary condition is imposed at both walls. The fundamental equations are the continuity and the Navier-Stokes equations without a compressibility effect.

The numerical method used in this study is the same as that used by Kim et al. (1987), and Iida et al. (1998). A spectral method is adopted with Fourier series in the x and z -directions and a Chebyshev polynomial expansion in the y -direction. The collocation grid used to compute the nonlinear terms in physical space has 1.5 times finer resolution to remove aliasing errors. For time integration, the second-order Adams-Bashforth and Crank-Nicolson schemes are adopted for the nonlinear and viscous terms, respectively.

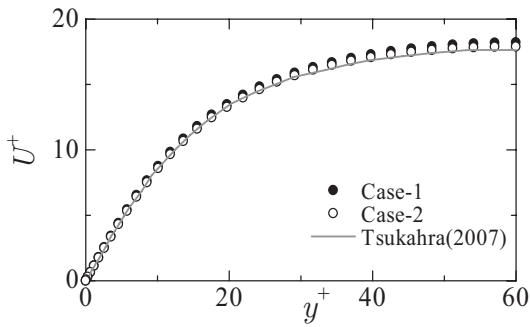


Figure 2: Mean velocity profiles. Case-1 and 2 represent results of different initial flow at same Reynolds number in present DNSs.

DNSs at $Re_\tau = 60$ are done in the computational domain of $L_x \times L_y \times L_z = 22\pi\delta \times 2\delta \times 10\pi\delta$ with $512 \times 65 \times 288$ grid points. We found no pile-up at high wave numbers in the energy and its dissipation spectra of all component of the velocity, indicating that the grid is adequately resolved in our numerical simulations. As the initial condition, fully developed Poiseuille flow is calculated in advance, and the Reynolds number Re_τ of the flow is systematically decreased to 60. The superscript + represents normalization using friction velocity u_τ over the entire channel and kinematic viscosity ν .

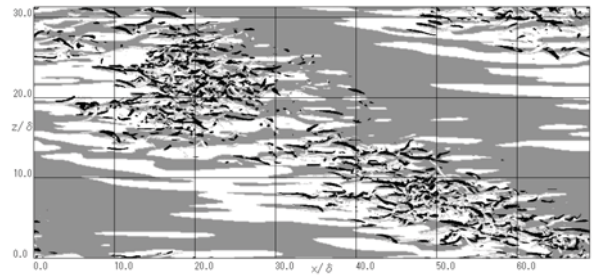
RESULTS AND DISCUSSION

Figure 2 shows the mean velocity profiles at $Re_\tau = 60$. The numerical result obtained by the different numerical code in different resolution is also included (Tsukahara et al., 2007). These data are in good agreement with each other, indicating the validity of our numerical code and results. Moreover, it is also noted that difference in the initial flow does not affect the mean velocity profile.

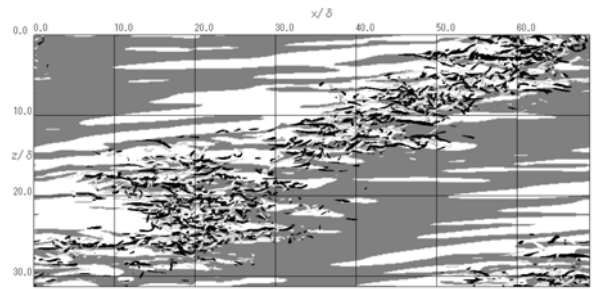
Figures 3 (a) and (b) show the longitudinal vortical structures and low-speed streaks in upper- and lower-wall sides in the same flow, respectively. The mean velocity profile of this flow is represented as Case-1 in Fig. 2. In both (a) and (b), each side of a channel is viewed from the channel centre, and hence the direction of the mean velocity gradient becomes identical.

It is noted that quasi-laminar and turbulent regions appear simultaneously in both sides, and that a flow becomes spatially intermittent. In the quasi-laminar region, longitudinal vortices represented by black and white isosurfaces, are rarely observed, while the turbulent region is featured by clustered longitudinal vortices. In contrast, the low-speed streaks in the quasi-laminar region tend to be extremely long and less curving compare to those in the turbulent region. Moreover, flow structure of the turbulent region is coherent and organized over more than $t^+ = 2000$, though not shown here.

It is also noted that in both sides of a channel, the turbulent region is inclined about an angle of 25 degree in the x - z plane with respect to the streamwise direction. However, this inclination angle becomes opposite between

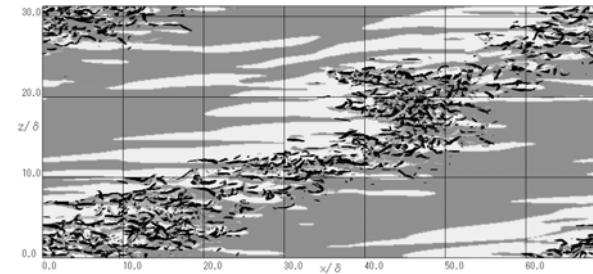


(a) Perspective of upper-wall side from channel center.

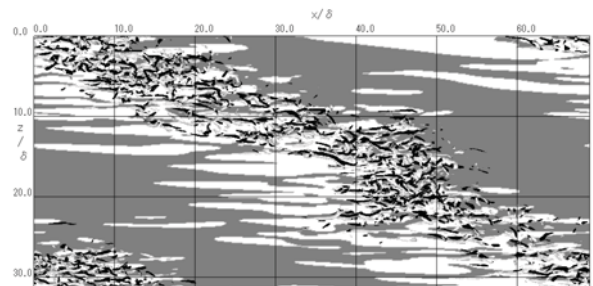


(b) Perspective of lower-wall side from channel center.

Figure 3: Instantaneous distribution of low-speed streaks and quasi-streamwise vortices in flow of Case-1. Gray represents $u^{t+} < 0$ at $y^+ \approx 10$, while both black and light-gray iso-surfaces are $II^+ = -u_{i,j}^{t+} u_{i,j}^{t+} = 0.005$.



(a) Perspective of upper-wall side from channel center.



(b) Perspective of lower-wall side from channel center.

Figure 4: Same as Fig. 2, though flow is Case-2.

the different sides of a channel, when the direction of mean velocity gradient is set to be identical in both sides.

Figure 4 shows the structures of the flow represented by Case-2 in Fig. 2, which has the same Reynolds number

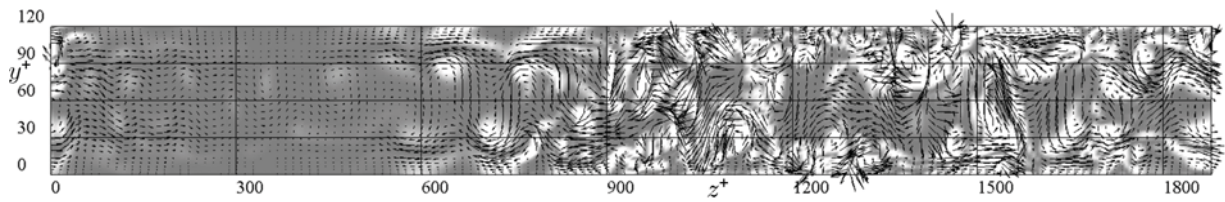


Figure 5: Instantaneous velocity vectors (v', w'), and distribution of instantaneous streamwise vorticity at the cross streamwise plane of $x/\delta \approx 15$ in the same flow as Fig. 3. Gray to white, $\omega_x^{+2} = 0$ to 0.01. The superscript $'$ represents fluctuating component.

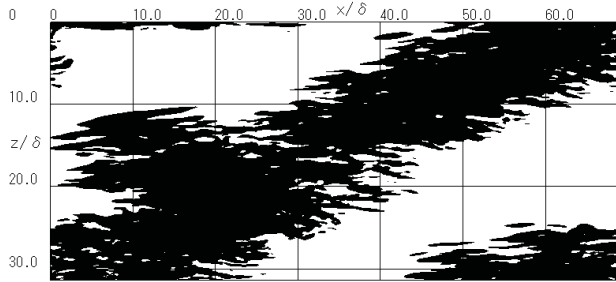


Figure 6: Division of turbulent and quasi-laminar regions by Eq. (2) in figure 2(b). Black region satisfying Eq. (2) represents the turbulent region, while white represents the quasi-laminar region.

as Fig. 3. Both flows are congruent, but mirror symmetric; in Figs. 3 and 4, the turbulent regions are inclined in the opposite direction.

Figure 5 shows velocity vectors and distribution of square of streamwise vorticity in the cross streamwise plane $x/\delta \approx 15$ in Figs. 3. In Fig. 5, quasi-laminar and turbulent regions are definitely observed in $z^+ < 750$ and $z^+ > 750$, respectively. The turbulent region is extended over the entire depth of a channel. Hence, it is confirmed that turbulent region is well correlated between different sides of a channel, as is obvious in the previous figures.

Moreover, it is also noted that in the turbulent region, the wall-normal velocity reaches opposite side of a channel across its center. In contrast, in quasi-laminar region, there are regularly arrayed streamwise vortices in the channel center, though their velocities are much smaller than those in the turbulent region. The vortices in channel center may produce the Reynolds stresses and develop the low-speed streaks.

We determine the criteria to distinguish between quasi-laminar and turbulent regions to discuss the statistical characteristics of them. As mentioned before, the turbulent and quasi-laminar regions are characterized as many clustered streamwise vortices and their scarcity, respectively. Hence, we use a streamwise vorticity as a useful criterion in the following.

First, the covariance of streamwise vorticity is locally calculated, and then it is averaged in the wall-normal direction from the bottom to top of a channel, followed by its square root as

$$\omega_{x \text{ rms}} \equiv \sqrt{\int_{-\delta}^{\delta} \omega_x^2 dy / 2\delta}. \quad (1)$$

In Eq. (1), $\omega_{x \text{ rms}}$ is expressed as a function of x and z . Moreover, the spatial average of $\omega_{x \text{ rms}}$ is calculated over the entire channel, and defined as $\overline{\omega_{x \text{ rms}}}$. Finally, the

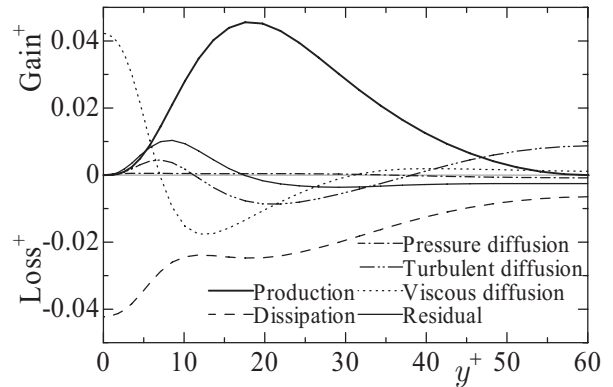


Figure 7: Budget of turbulent kinetic energy at quasi-laminar region.

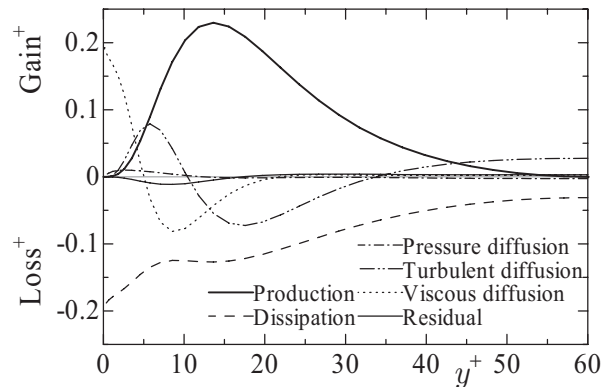


Figure 8: Budget of turbulent kinetic energy at turbulent region.

turbulent region is classified as the region satisfying the following condition,

$$\omega_{x \text{ rms}} \geq C \overline{\omega_{x \text{ rms}}}. \quad (2)$$

In this study, the constant C is determined to be 0.6. Regions satisfying Eq. 2 are represented as black in Fig.6, and corresponding very well to turbulent region including many streamwise vortices as shown in Fig. 3(b). Hence, the criteria of Eq. 2 must be a good working definition to distinguish different flows.

Figures 7, 8 show budget of turbulent kinetic energy averaged in quasi-laminar and turbulent regions, respectively. In quasi-laminar region, all the terms in the budget become small over the entire channel, and the peak location of each term tends to shift to channel center in comparison to those in turbulent regions, though their distributions are quite similar in both regions. The Reynolds stresses are still

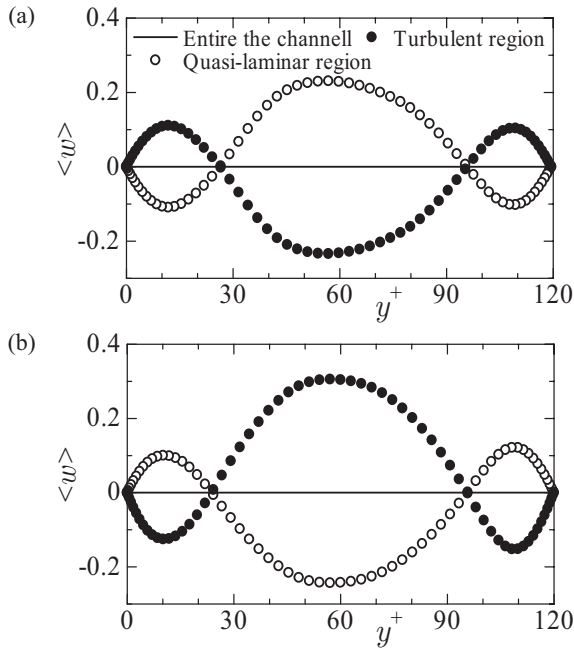


Figure 9: Mean values of spanwise velocity in quasi-laminar and turbulent regions, entire the channel. (a) and (b) are results of same instantaneous flow as Fig. 2 and 3, respectively. $\langle \cdot \rangle$ represents mean value in each region.

produced in the quasi-laminar region due to existing of the production term. It is also noted that there is no-negligible amount of residuals in both regions, though their signs are opposite between two regions. We confirmed that the residual becomes zero in the budget averaged over the entire channel, though not shown here. Hence, the residual must be generated because the quasi-laminar and turbulent regions are spatially divided, and these two regions are interacted with each other; turbulent kinetic energy must be exchanged between two different regions.

It is noted from the residual of Figs. 7 and 8 that in the region $y^* > 17$, turbulent kinetic energy is transferred from quasi-laminar to turbulent region, while it is transferred from turbulent to quasi-laminar region in very near-wall region of $y^* < 17$. The above mentioned energy exchange between the two different regions makes the flow almost steady, which results in the two regions appearing simultaneously in the same computational domain. It is also obvious that the energy exchange between two regions is attributed to the tilting of turbulent region with respect to the streamwise direction, which generates interface between both regions along the streamwise direction.

Next, we discuss the large-scale flow associated with each region, which can be elucidated as a mean value there. Figure 9 shows locally and entirely averaged values of spanwise velocity, while Figs. 10 and 11 are those of streamwise and wall-normal vorticities, respectively. In all figures, three different averages, i.e., those over the entire channel, turbulent region and quasi-laminar region, are compared with one another, though the average over the entire channel is zero.

As shown in Fig. 9, mean spanwise velocities in both

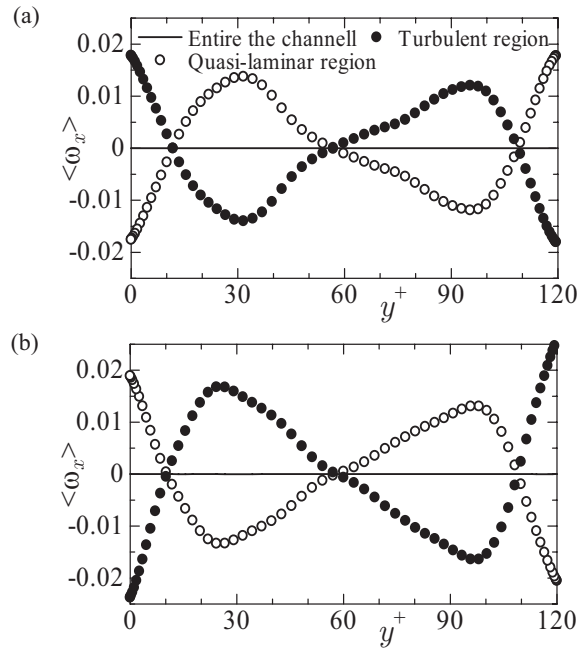


Figure 10: Mean values of streamwise vorticity in quasi-laminar and turbulent region, entire the channel. (a) and (b) are same as those of Fig. 9.

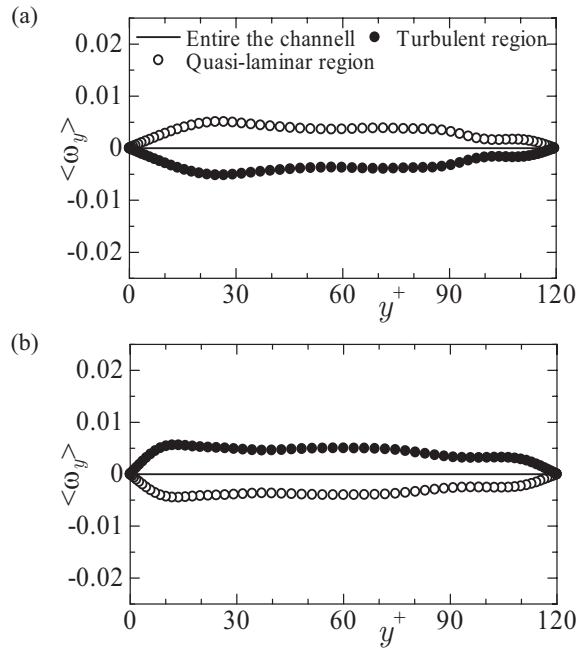


Figure 11: Mean values of wall-normal vorticity in quasi-laminar and turbulent region, entire the channel. (a) and (b) are same as those of Fig. 9.

quasi-laminar and turbulent regions are symmetric, strongly indicating that their no-zero values are not due to the statistical error, but to the large-scale flow related to each region. Interestingly, the sign of mean value is reversed between two different flows with opposite inclination angle of turbulent region, which is also true in the mean streamwise and wall-normal vorticities as shown in Figs. 10 and 11.

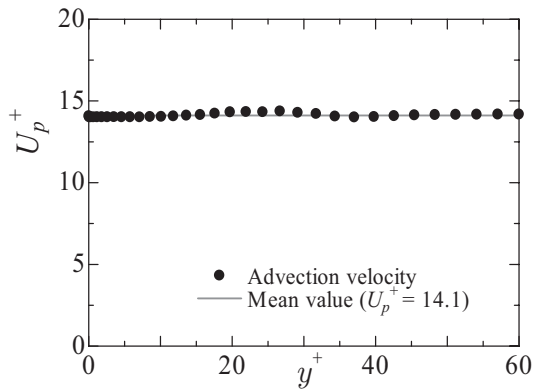


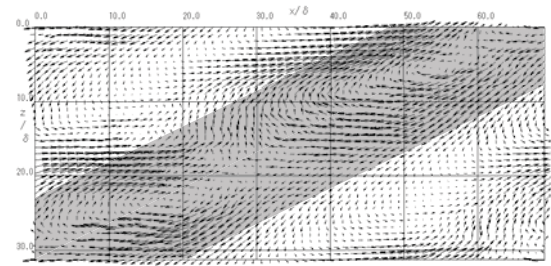
Figure 12: Distribution of advection velocity.

It also should be noted that although signs of mean spanwise velocity are identical between two different sides of a channel, which have turbulent regions with different inclination angle, they must become exact opposite when the directions of coordinate system are set to be identical. This is also true in the mean value of wall-normal vorticity. Hence, the sense of inclination angle of turbulent region is strongly related to the sign of mean values of spanwise velocity, and streamwise and wall-normal vorticities, which mechanisms is discussed in detail by visualizing the averaged structure of turbulent region over time.

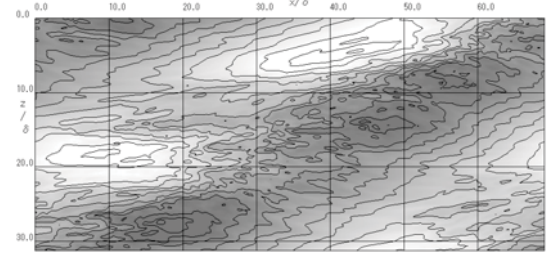
By visualizing the time development of the flow, we found that turbulent region is floated downstream with almost the same outline, which strongly indicates that the advection velocity has a unique value over the entire depth of a channel. Then, the advection velocity was estimated in the following. First, we calculated the spatial correlation coefficient R_{uu} of streamwise velocity fluctuations at the two x - z planes of the same y location, but at different times. Then, two planes were shifted from each other by a distance dx in the streamwise direction, and their correlation coefficient was calculated again as a function of dx and the time difference dt . Finally, relation between dt and dx was investigated when R_{uu} took the local maximum, and approximated as a linear function, which slope was defined as the advection velocity at the y location. Figure 12 shows the distribution of advection velocity obtained by the procedure mentioned above. It is noted that the advection velocity takes almost the constant value, and equals 14.1, which is a bit larger than 13.8, a value of mean bulk velocity. Finally, the turbulent regions were pinned down by subtracting their advection velocity from the mean flow, and their spatial statistics were averaged with time every time interval $\Delta t^+ = 6.0$ over $t^+ = 1200$.

Figure 13(a) shows thus averaged velocity vectors (\tilde{u}, \tilde{w}) in the plane parallel to the wall, where $\tilde{\cdot}$ represents the time average of streamwise and spanwise velocity fluctuations, respectively. It is noted in Fig. 13(a) that two large-scale vortices with negative wall normal vorticity are generated in the turbulent region.

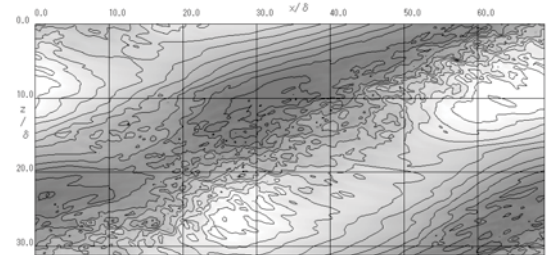
Figures 13(b) and (c) show distribution of \tilde{u} and \tilde{w} , respectively. It is noted in Fig. 13(b) that the high- and



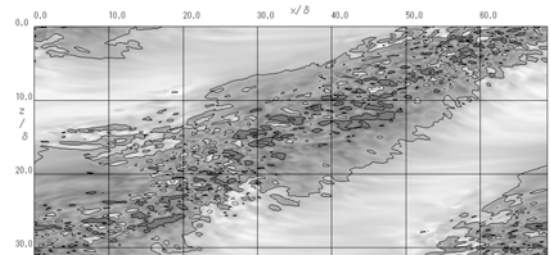
(a) Velocities (\tilde{u}, \tilde{w}) in x - z plane of channel center. Light-gray region represents turbulent region.



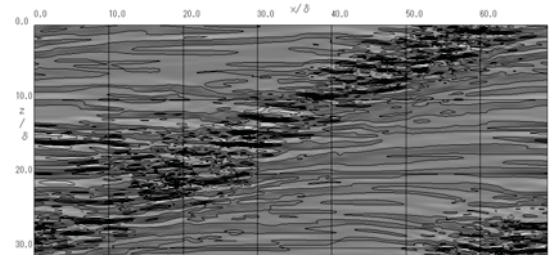
(b) \tilde{u} in same x - z plane as (a). Dark gray to white; -2 to 2. Counter interval 0.5.



(c) \tilde{w} in same x - z plane as (a). Dark gray to white; -1 to 1. Counter interval 0.2.



(d) Averaged streamwise vorticity $\tilde{\omega}_x$ at $y^+ = 30$. Dark gray to white; -0.05 to 0.05. Counter interval 0.05.



(e) Averaged wall-normal vorticity $\tilde{\omega}_y$ at $y^+ = 10$. Dark gray to white; -0.05 to 0.05. Counter interval 0.05.

Figure 13: Flow field of Case-1 conditionally averaged over time. $\tilde{\cdot}$ represents the averaged mean values.

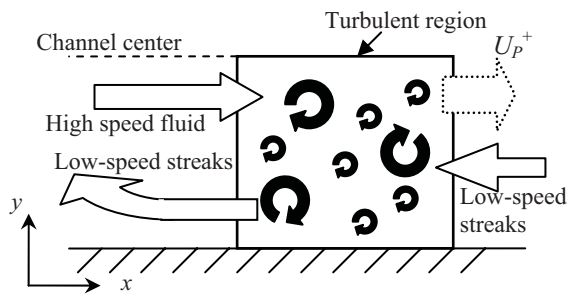


Figure 14: Schematics of the energy exchange between quasi-laminar and turbulent regions.

low-speed fluids are located at upstream and downstream of the turbulent region, respectively, as observed in Figs 2 and 3. The regions where \tilde{u} and \tilde{w} take large values are well correlated to the large-scale vortices observed in Fig. 13(a). Hence, it is again confirmed that the turbulent region is featured by the large-scale vortices circulating the region. Moreover, it is also noted that at turbulent region at the channel centre, spanwise velocity takes the negative value as indicated by Fig. 9(a).

Figure 13(d) shows averaged streamwise vorticity $\tilde{\omega}_x$ at $y^+=30$. It is noted that $\tilde{\omega}_x$ becomes negative in the entire turbulent region, which is in good agreement with Fig. 10(a); the region of the negative streamwise vorticity is very well correlated with the turbulent region. The close correlation between Figs. 13(c) and (d) shows that mean streamwise vorticity is attributed to mean spanwise velocity striding the turbulent region at the channel centre.

Figure 13(e) shows averaged wall-normal vorticity $\tilde{\omega}_y$ at $y^+=10$, which is not well correlated to the turbulent region in comparison to $\tilde{\omega}_x$. However, it is well associated with low-speed streaks especially in the quasi-laminar region, indicating the robustness of low-speed streaks there.

Finally, we will discuss how the large-scale flow structures are related to the exchange of turbulent kinetic energy between the two regions. Figure 14 shows the schematics of energy exchange between quasi-laminar and turbulent regions. As is previously indicated, the advection velocity of turbulent region can be assumed to be constant over the entire channel, and equals mean streamwise velocity at $y^+ \approx 22$. Hence, at the region away from the wall, especially at the channel center, the turbulent region is floated slower than the quasi-laminar region behind, and hence impinged by the latter, which is well represented in Fig. 13(a). In contrast, near the wall the low-speed streaks generated in the turbulent region is left behind, and hence garnered in the quasi-laminar region. Although the result is not shown here, the low-speed streaks left behind are lifted upward later in the quasi-laminar region, and finally absorbed by the upstream turbulent region.

CONCLUSIONS

Direct numerical simulations are carried out to investigate turbulent structures in relaminarizing turbulent

Poiseuille flow at very low-Reynolds number. The flow, simultaneously including quasi-laminar and turbulent regions, becomes spatially intermittent. Our findings are recapitulated below.

1. Turbulent region is inclined about an angle of 25 degree in the plane parallel to the wall with respect to the streamwise direction. Difference in the initial flow results in the opposite inclination angle, and the entire flow becomes mirror symmetric.
2. In the turbulent region, wall-normal flow is generated to stride over channel center, and the different side of a channel are interacted with each other. In quasi-laminar region, however, regularly arrayed streamwise vortices are generated in the channel centre.
3. By using the streamwise vorticity as criterion, quasi-laminar and turbulent regions are adequately distinguished from each other, and budget of the turbulent kinetic energy is calculated in each region. As a result, we find the definite energy exchange between quasi-laminar and turbulent regions, which is attributed to the tilting of turbulent region with respect to the streamwise direction, and generation of the interface between two regions along the streamwise direction.
4. By averaging turbulent region over time, we find that turbulent region is featured by large-scale flows circulating around the turbulent region in the plane parallel to the wall. It is also found the mean streamwise vorticity well correlated to the entire turbulent region.
5. The advection velocity of turbulent region can be assumed to be constant over the entire channel, Hence, at the region away from the wall, the turbulent region is floated slower than the quasi-laminar region behind, and hence impinged by the latter. In contract, near the wall the low-speed streaks generated in the turbulent region is left behind, and hence garnered in the quasi-laminar region.

REFERENCES

- Barkley, D. & Tuckerman, L., 2007 Mean flow of turbulent-laminar patterns in plane couette flow, *J. Fluid Mech.*, Vol. 576, pp. 109-137.
- Fukudome, K., Iida, O., and Nagano, Y., 2008 The turbulent structures of Poiseuille flows at low-Reynolds numbers, *Proceedings, 7th JSME-KSME Thermal and Fluid Engineering Conference*, Sapporo, K112,
- Iida, O. & Nagano, Y., 1998 The relaminarization mechanisms of turbulent channel flow at low Reynolds numbers, *Flow, Turbulence and Combustions* ., Vol. 60, pp. 193-213.
- Kim, J., Moin, P. & Moser, R., 1987 Turbulence statistics in fully developed channel flow at low Reynolds number, *J. Fluid Mech.*, Vol. 177, pp. 133-166.
- Tsukahara, T., 2007, Study of turbulent structure through large-scale DNS of turbulent channel and Couette flows at low-Reynolds numbers (in Japanese), Doctor Thesis, Tokyo University of Science